

Raman scattering in GaAs/AlAs superlattices with Fibonacci structure

G. Wahlström and K. A. Chao

Department of Physics and Measurement Technology, University of Linköping, S-581 83 Linköping, Sweden

(Received 19 October 1988; revised manuscript received 9 January 1989)

We have used a one-dimensional model to calculate the phonon spectra of quasiperiodic Fibonacci superlattices either with a perfect sharp interface or with imperfection. An analytical prediction for peak positions of Raman backscattering with a scattering geometry $z(x,x)\bar{z}$ was derived and confirmed by an exact numerical computation in the region of long wavelengths. The calculated Raman spectrum agrees extremely well with the experimental data of Nakayama *et al.* Critical phonon modes are found in the frequency region near the upper edge of the longitudinal-acoustical branch, and can be destroyed easily by very weak imperfection. Our calculation suggests the requirement of a very-high-quality sample in order to detect the interesting properties of such critical states associated with the Fibonacci structure.

I. INTRODUCTION

The absence of translational invariance in a quasiperiodic system leads to the hierarchical splitting of energy spectra for both electrons¹ and phonons.² The electronic properties and the lattice dynamics of such systems have been studied by many authors³⁻¹² using a one-dimensional tight-binding Hamiltonian or the modulated Kronig-Penney model. Theoretical predictions of certain novel properties of one-dimensional quasiperiodic systems can hardly be confirmed by experiments. However, one successful case is the optical transmission of Rb_2ZnBr_4 , where the calculated spectra¹¹ exhibit the characteristic features of experimental observations.¹⁰

The development of molecular-beam-epitaxy (MBE) techniques provides the opportunity to check many theoretical results on interesting physical properties of one-dimensional quasiperiodic systems. Semiconductor superlattice crystals with layer thicknesses modulated along one crystal axis can be fabricated with the MBE.¹³ Assuming a periodic modulation with period incommensurate to that of the underlying superlattice, Das Sarma *et al.*¹⁴ suggested the detection of localized states in an incommensurate structure via the plasma excitations. Hawrylak *et al.*¹⁵ have studied the so-called critical plasmon states for superlattice with a modulation following a Fibonacci sequence.

However, the existing direct experimental investigation on Fibonacci-modulated semiconductor superlattices is to probe phonon spectra via Raman scattering.^{13,16-18} In this paper we present a theoretical calculation of the Raman spectra and compare our results with available experiments. The model, based on which the theory of Raman scattering will be established in Sec. III, will be described in Sec. II. In the long-wavelength region we derive an analytical expression for the positions of the main Raman peaks in Sec. IV, and check its accuracy with exact numerical calculation. In Sec. V our calculated spectrum is compared with experimental data, demonstrating excellent agreement. The effect of imperfections of the sample is investigated in detail, and its influence on

the possibility of observing Fibonacci characteristics will be discussed in the Sec. VI.

II. THE MODEL

To the advantage of both experimental investigation and theoretical analysis, GaAs/AlAs superlattice samples are usually grown along the [001] axis. Modern MBE techniques can control the total thickness of each constituent semiconductor within an error of less than one monolayer ($\approx 2.8 \text{ \AA}$).¹⁸ With such experimental accuracy, quasiperiodic superlattices have been fabricated to specifications. Instead of alternately repeating the basic building blocks A and B [for example, A can be $(\text{GaAs})_\mu$ and B can be $(\text{AlAs})_\nu$] of the two constituent materials in a periodic array, A and B can appear to be arranged in some other exotic fashion. Quasiperiodic Fibonacci superlattices have been grown with constituent transition metals Mo/V (Ref. 19) and strain-layered semiconductors Si/Ge_xSi_{1-x},²⁰ besides the GaAs/AlAs (Refs. 13 and 16-18) of our current interest.

Construction of Fibonacci sequence with basic building blocks A and B is defined by concatenation via the recursion relation $S_{l+2} = S_{l+1}S_l$ for $l \geq 1$, with $S_1 = A$ and $S_2 = AB$. Since we are interested at present in the GaAs/AlAs system, our quasiperiodic Fibonacci superlattice (QPFSL) is defined by specifying $A = (\text{GaAs})_\mu / (\text{AlAs})_\nu$, and $B = (\text{GaAs})_\gamma / (\text{AlAs})_\tau$.

An ideal superlattice has perfect sharp interfaces and no fluctuation in the thicknesses of each constituent layer. However, this is not the case in reality. Because the lattice vibration depends strongly on the nearest-neighbor elastic force, the phonon modes are very sensitive to imperfections of the superlattice. With use of a continuum model, the long-wavelength phonon modes of a QPFSL have been studied.^{13,16,18} Since the continuum model is invalid for high-frequency phonon modes, in this paper we will instead use a discrete model.²¹⁻²³

Barker *et al.*²² have shown that for wave vectors parallel to the [001] direction, the transverse and the longitudinal vibrations are decoupled because they belong to

different group representations. Hence, to analyze the Raman backscattering by longitudinal phonons along the [001] direction, it is sufficient to consider a discrete chain of atoms whose positions coincide with the projected positions of all atoms on the [001] axis, which is defined as the z axis. Let U_i be the displacement of the i th atom from its equilibrium position on the linear chain, M_i the mass of the i th atom, and $K_{i,i+1}$ the force constant between the i th and the $(i+1)$ th atoms. Then, in harmonic approximation the equation of motion of the i th atom is

$$M_i d^2 U_i / dt^2 = -K_{i-1,i} (U_i - U_{i-1}) - K_{i,i+1} (U_i - U_{i+1}). \quad (1)$$

There are two different values of elastic constant: one for the Ga—As pair and the other for the Al—As pair. Since these two elastic moduli are almost identical,²¹ we will adopt a single value $K_{i,i+1} = K$ for all i . To simplify the algebraic manipulation involved in numerical solutions of (1), we will normalize the phonon energy by setting the force constant $K=1$, the mass of As atom $M_{\text{As}}=1$, and the lattice constant $a=1$. Then, the mass of the Ga atom and the Al atom are, respectively, $M_{\text{Ga}}=0.93057$ and $M_{\text{Al}}=0.36013$.

Although (1) can be solved numerically for a QPFSL constructed from arbitrary building blocks $A=(\text{GaAs})_\mu/(\text{AlAs})_\nu$ and $B=(\text{GaAs})_\gamma/(\text{AlAs})_\tau$, we will solve (1) for a specific structure with $\mu=\nu=\gamma=10$ and $\tau=0$, for which detailed Raman backscattering data are available.¹⁸ The thicknesses of the QPFSL samples used in experiments correspond to either the 13th or the 14th generation in the Fibonacci construction. That is, when the samples are generated by concatenation via the recursion relation $S_{l+2}=S_{l+1}S_l$, for $l \geq 1$, with $S_1=A$ and $S_2=AB$ the last block S_η is the 13th or the 14th of the whole sequence ($\eta=13$ or 14). Hence, each measured sample consists of typically about 10^4 monolayers of GaAs and AlAs. [In particular, in the ideal case there will be 6100 and 9870 “monolayers” (of GaAs and AlAs) for the 13th- and 14th-generation FSL, respectively.] For such sample length, exact numerical solutions of (1) can

be easily derived with modern computational techniques.

In our energy units the top of the longitudinal-acoustical branch has the value $(2K/M_{\text{As}})^{1/2} = \sqrt{2}$. The corresponding measured value is 201 cm^{-1} . Since lattice vibration with long wavelength is insensitive to the local structure, the effect of Fibonacci modulation on phonon modes may manifest itself more in the high-frequency region of the spectrum, and hence can be detected by Raman backscattering.

The only additional approximation in our model calculation is the use of a single force constant $K_{i,i+1}=K$ for all pairs of nearest neighbors. To be precise, the force constant of pure AlAs is slightly larger than that of pure GaAs.²² Therefore, in the vicinity of the top edge of the longitudinal-acoustical branch, phonons propagate in AlAs layers but weakly decay exponentially in GaAs layers. Such influence may interfere with the expected strong effect of quasiperiodicity on phonon modes in this energy region. In later sections we will return to this point for details.

III. RAMAN SCATTERING

A complete description of the theory of Raman scattering has been presented by Born and Huang.²⁴ In this section we will only outline the key points and then use the bond-polarizability approximation^{22,23,25,26} to calculate the backscattering from a QPFSL sample. However, we should mention that He *et al.*²⁷ have argued that a correct description of Raman intensities scattered by longitudinal-acoustic phonons requires the coupled solution of Maxwell's equations in the superlattice.

Consider a polarizable medium under an electric field

$$\mathbf{E}(\mathbf{r}) = \mathbf{E}^- \exp[-i\omega_i t + 2\pi i n(\mathbf{r}) \hat{\mathbf{k}} \cdot \mathbf{r} / \lambda] + \mathbf{E}^+ \exp[i\omega_i t - 2\pi i n(\mathbf{r}) \hat{\mathbf{k}} \cdot \mathbf{r} / \lambda], \quad (2)$$

where $n(\mathbf{r})$ is the local refractive index, $\mathbf{E}^- = (\mathbf{E}^+)^*$ an arbitrary constant vector, and the wavelength λ is much longer than the lattice constant. The induced local electric moment $\mathbf{m}(\mathbf{r}, t)$ associated to the transition between two eigenstates $|\mu\rangle$ and $|\nu\rangle$ can be expressed as

$$m_\alpha(\mathbf{r}, t) = \sum_B \{ \langle \mu | P_{\alpha\beta}(\mathbf{r}) | \nu \rangle^* E_\beta^- \exp[2\pi i n(\mathbf{r}) \hat{\mathbf{k}} \cdot \mathbf{r} / \lambda - i(\omega_i + \omega_{\mu\nu})t] + \langle \mu | P_{\alpha\beta}(\mathbf{r}) | \nu \rangle E_\beta^+ \exp[-2\pi i n(\mathbf{r}) \hat{\mathbf{k}} \cdot \mathbf{r} / \lambda + i(\omega_i + \omega_{\mu\nu})t] \} \quad (3)$$

for $\alpha, \beta = x, y, z$. $\hbar\omega_{\mu\nu}$ is the difference of the two corresponding eigenenergies, and $P_{\alpha\beta}(\mathbf{r})$ is the (α, β) component of the polarizability tensor.

Since we are interested in the backscattering along the z axis which lies in the [001] direction of a discrete lattice, $\hat{\mathbf{k}}$ is parallel to $\hat{\mathbf{z}}$ and $\hat{\mathbf{k}} \cdot \mathbf{r} = j$, where j labels the projection of the atomic position on the z axis. Furthermore, the experimental data to be compared with our calculation are obtained with the scattering geometry $z(xz)\bar{z}$. That is, both incident and scattered electric fields propagate parallel to the z axis and are polarized along the x

axis. The frequency ω_i of the incident laser beam is much higher than $\omega_{\mu\nu}$ and hence we can neglect the $\omega_{\mu\nu}$ in (3). Under such condition, (3) reduces to

$$m_x(j, t) = \langle \mu | P_{xx}(j) | \nu \rangle^* E_x^- \exp[2\pi i j n(j) / \lambda - i\omega_i t] + \langle \mu | P_{xx}(j) | \nu \rangle \times E_x^+ \exp[-2\pi i j n(j) / \lambda + i\omega_i t]. \quad (4)$$

The total electric moment of the system $M_x(t)$ is the sum of all local moments $m_x(j, t)$ over j . However, from

different atoms the scattered lights reach the detector at different times. Taking into account this retardation effect and approximating the local refractive index $n(j)$ by its average value n , the time t in (4) must be replaced by $t - jn/c$, where c is the speed of light. We then obtain the total electric moment of the QPFSL sample as

$$M_x(t) = \left[\sum_j \langle \mu | P_{xx}(j) | \nu \rangle \exp(-2ij\omega_i n/c) \right]^* \times E_x^- \exp(-i\omega_i t) + \left[\sum_j \langle \mu | P_{xx}(j) | \nu \rangle \exp(-2ij\omega_i n/c) \right] \times E_x^+ \exp(i\omega_i t). \quad (5)$$

The above expression is the same as Eq. (19.16) in Ref. 24 except for the additional phase factor $\exp(-2ij\omega_i n/c)$ due to the retarded-time effect. Therefore, the intensity of Raman scattering due to the transition between two vibrational states $|\mu\rangle$ and $|\nu\rangle$ is given by Eq. (49.1) in Ref. 24 as

$$J(\omega_s) = (\omega_s^4 / 2\pi c^2) I_{xx,xx}(\omega) E_x^- E_x^+, \quad (6)$$

where ω_s is the frequency of Raman scattered light, and the Raman tensor $I_{xx,xx}(\omega)$ of frequency $\omega = \omega_i - \omega_s$ has the form

$$I_{xx,xx}(\omega) = \left\langle \left\langle \left[\sum_j \langle \mu | P_{xx}(j) | \nu \rangle \times \exp(-2ij\omega_i n/c) \right] \right|^2 \right\rangle_{av}. \quad (7)$$

In the above equation $\langle \dots \rangle_{av}$ is the thermal average over the initial vibrational state.

The polarizability tensor $\mathbf{P}(\mathbf{r})$ will be calculated in the bond-polarizability approximation,^{22,23,25,26} by which each bond contributes independently to the total polarizability. We start with a general three-dimensional system and let $\mathbf{r}_i = \mathbf{R}_i + \mathbf{U}_i$ be the instantaneous position of the i th atom, where \mathbf{U}_i is the displacement from the equilibrium position \mathbf{R}_i . To each bond of the $\langle ij \rangle$ pair of atoms separated by $\mathbf{r}_{ij} = \mathbf{r}_i - \mathbf{r}_j$, there is an axially symmetric bond polarizability $\mathbf{P}(\mathbf{r}_{ij})$. If $\bar{\mathbf{P}}(\mathbf{r}_{ij})$ is the mean polarizability and $\gamma(\mathbf{r}_{ij})$ the anisotropy, we can then write

$$\mathbf{P}(\mathbf{r}_{ij}) = \bar{\mathbf{P}}(\mathbf{r}_{ij}) \cdot \mathbf{I} + \gamma(\mathbf{r}_{ij})(\hat{\mathbf{r}}_{ij} \hat{\mathbf{r}}_{ij} - \frac{1}{3} \mathbf{I}), \quad (8)$$

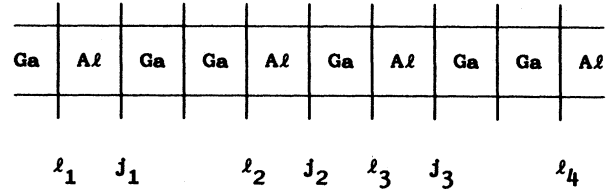
where $\hat{\mathbf{r}}_{ij} = \mathbf{r}_{ij}/r_{ij}$, and \mathbf{I} is a unit tensor.

Since the relative displacement $|\mathbf{U}_i - \mathbf{U}_j|$ is much smaller than the equilibrium distance $|\mathbf{R}_i - \mathbf{R}_j|$, we can expand $\mathbf{P}(\mathbf{r}_{ij})$ in powers of $|\mathbf{U}_i - \mathbf{U}_j|$ and keep only the linear term. The algebraic manipulations are very lengthy and have been worked out in Ref. 23. Here we only quote the final results. Let us divide the QPFSL into cubes, each of which is demonstrated in Fig. 1(c) of Ref. 23. The atom at the center of the cube (marked by A) is either an Al atom or a Ga atom, and the four atoms at the corners of the cube (marked by $B_1, B_2, B_3,$ and B_4) are As atoms. The four bonds connecting the center atom and the four corner atoms are identical, and so the corresponding bond-polarizability tensors have similar

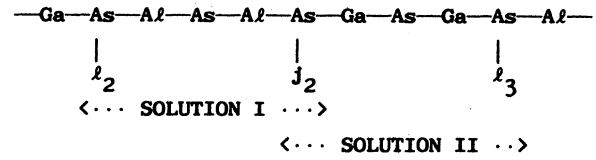
structure. We have mentioned earlier that in a longitudinal-acoustical mode, all atoms in a single (001) plane vibrate as a whole. For such modes, we only need the contributions to bond-polarizability tensors from longitudinal displacements which have the same value for all atoms in one (001) plane. The net contribution to the total polarizability tensor from all four bonds in one cube is then linear in z components of the relative displacements of the corner As atoms with respect to the center Ga or Al atom (linear in $U_{0z} - U_{iz}$ with $i=1,2,3,4$).

The explicit expression of the bond polarizability of one cube is given by Eqs. (8) and (10) in Ref. 23. If we define \mathbf{S} as the set of Ga and Al atoms in the linear-chain model system, then the Raman tensor for the $z(xx)\bar{z}$ scattering geometry can be expressed as

$$I_{xx,xx}(\omega) = \left\langle \left\langle \left[\sum_{j \in \mathbf{S}} \alpha_{xx,j} \langle \mu | (U_{j+1} - U_{j-1}) | \nu \rangle \times \exp(-2ij\omega_i n/c) \right] \right|^2 \right\rangle_{av}, \quad (9)$$



(a)



(b)

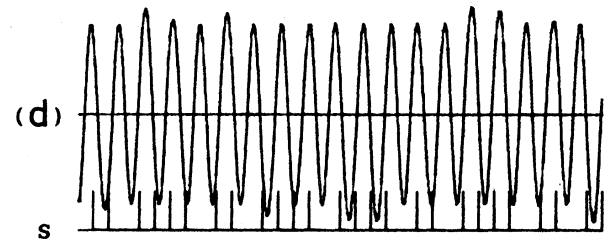
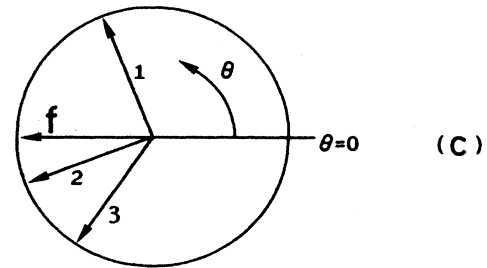


FIG. 1. Schematical description of the computation procedure used in Sec. III. See text for details.

where $j \in S$ means that j belongs to the set S , and the parameter $\alpha_{xx,j}$ is defined by Eq. (9a) in Ref. 23. Depending on the kind of atom (Ga or Al) at the j th position, $\alpha_{xx,j}$ can have two values.

The matrix element $\langle \mu | (U_{j+1} - U_{j-1}) | \nu \rangle$ in (9) can be calculated using the phonon modes (or normal coordinates) of (1). Let $\{|q_l\rangle\}$ be the normalized complete set of longitudinal-acoustic modes with associated eigenenergies $\{\hbar\omega_l\}$. The displacement U_j can then be expressed as

$$U_j = [1/(M_j)^{1/2}] \sum_l \xi_{jl} |q_l\rangle, \quad (10)$$

where ξ_{jl} is the j th component of the l th phonon mode $|q_l\rangle$. When (10) is substituted into (9), the matrix element $\langle \mu | q_l | \nu \rangle$ will be finite only if $\omega_l = \pm\omega_{\mu\nu}$. Equation (9) can now be cast into the form

$$I_{xx,xx}(\omega_l) = \left| \sum_{j \in S} \alpha_{xx,j} (\xi_{j+1,l} - \xi_{j-1,l}) \exp(-2ij\omega_l n/c) \right|^2 \times \langle \langle |\langle \mu | q_l | \nu \rangle|^2 \rangle \rangle_{av}. \quad (11)$$

The thermal-averaged matrix elements are given in Sec. 16 of Ref. 24. For the Stokes component they are

$$\langle \langle |\langle \mu | q_l | \nu \rangle|^2 \rangle \rangle_{av} = (\hbar/2\omega_l) [1 - \exp(-\hbar\omega_l/k_B T)]^{-1}. \quad (12)$$

To avoid the divergence introduced by the factor $1/\omega_l$ as

$$R_{xx}(\omega) \approx \left| \sum_{j \in S} \alpha_{xx,j} \{ \xi_{j+1,\omega} \exp[-2i(j+1)\omega_l n/c] - \xi_{j-1,\omega} \exp[-2i(j-1)\omega_l n/c] \} \right|^2 [1 - \exp(-\hbar\omega/k_B T)]^{-1}. \quad (14)$$

Since the set S contains all Ga and Al atoms, the atoms at positions $j \pm 1$ are As atoms. Within the same constituent material, there is a large number of cancellations in the summation of (14) between terms $\alpha_{xx,j} \xi_{j+1,\omega}$ and $\alpha_{xx,j+2} \xi_{j+1,\omega}$ because $\alpha_{xx,j} = \alpha_{xx,j+2}$. Only for those As atoms which mark the interfaces between two constituent materials, the bond polarizabilities from both sides (one from Ga—As bond and the other from Al—As bond) will not cancel each other. Let us define $\alpha_{xx,Al}$ and $\alpha_{xx,Ga}$ the values of $\alpha_{xx,j}$ for the Al—As bond and the Ga—As bond, respectively. Equation (14) can then be simplified to

$$R_{xx}(\omega) = |\alpha_{xx,Al} - \alpha_{xx,Ga}|^2 \times \left| \left[\sum_{j \in R} - \sum_{j \in L} \right] \xi_{j,\omega} \exp(-2ij\omega_l n/c) \right|^2 \times [1 - \exp(-\hbar\omega/k_B T)]^{-1}, \quad (15)$$

where R (or L) is the set of As atoms on those interfaces with GaAs constituent material to the right-hand (or left-hand) side of the interface. The elements of the set R (or L) are shown in Fig. 1(a) as j_i (or l_i).

The numerical results presented in the next section are obtained with (15). In the rest of this section, we will further analyze (15) to give the theoretical prediction of the

ω_l approaches zero, we will instead calculate the Raman tensor component

$$R_{xx}(\omega) = (2\omega/\hbar) I_{xx,xx}(\omega) = \left| \sum_{j \in S} \alpha_{xx,j} (\xi_{j+1,\omega} - \xi_{j-1,\omega}) \times \exp(-2ij\omega_l n/c) \right|^2 \times [1 - \exp(-\hbar\omega/k_B T)]^{-1}. \quad (13)$$

We remind the reader that we have changed the labeling of the eigenmode from l to ω , and so $\xi_{j,l}$ is now expressed as $\xi_{j,\omega}$. It is clear that $R_{xx}(\omega)$ is proportional to $\omega J(\omega)$, where $J(\omega)$ is the intensity of Raman scattered light defined by (6).

IV. RAMAN TENSOR IN LONG-WAVELENGTH REGION

All approximating calculations in the region of the long wavelength are based on the condition that the phonon wavelength is much longer than the lattice constant a (in our case $a=1$). In the extreme limit of the continuum model, the coefficient $\xi_{j,\omega}$ has the form of a plane wave and the Raman intensity has been computed by many authors.^{13,18,20,21,28,29} For the discrete model considered here, we calculate $\xi_{j,\omega}$ from solving (1) numerically, but introduce the long-wavelength approximation through the phase factor by rewriting (13) as

positions of main Raman peaks. In each constituent material, the time-independent eigensolution of (1) has the general form

$$\xi_{j,\omega} = C_{\omega,j+} \exp[i\kappa(\omega)j] + C_{\omega,j-} \exp[-i\kappa(\omega)j], \quad (16)$$

where for given ω there are two values of $\kappa(\omega) \equiv \kappa_\eta$; κ_{Ga} for position j in GaAs and κ_{Al} for position j in AlAs. κ_η is determined by the boundary conditions at the interfaces as

$$\kappa_\eta = \frac{1}{2} \arccos \left[\frac{1}{2M_{AS}} (\omega^2 - 2)(M_\eta \omega^2 - 2M_{As}) - 1 \right], \quad \eta = \text{Ga, Al}. \quad (17)$$

Substituting (16) into (15), the summation can be divided into two parts

$$\left[\sum_{j \in R} - \sum_{j \in L} \right] \xi_{j,\omega} \exp(-2ij\omega_l n/c) = \Xi_+(\omega) + \Xi_-(\omega),$$

where

$$\Xi_\pm(\omega) = \sum_{j \in R} C_{\omega,j\pm} \exp[i(\pm\kappa_{Al} - q)j] - \sum_{l \in L} C_{\omega,l\pm} \exp[i(\pm\kappa_{Ga} - q)l] \quad (18)$$

with $q \equiv 2\omega_i n/c$.

To continue our analysis we need to know the amplitudes $C_{\omega, j\pm}$ and $C_{\omega, l\pm}$ of the As atoms at the interfaces. The general procedure of solving (1) is as follows. Let us first consider an infinite chain of GaAs for which the general solution is given by (16) and (17). The wave traveling to the right and the left are indicated by superscripts \pm as

$$U_j = G_{\omega, \eta}^{\pm} \exp(\pm i\kappa_{\text{Ga}} j - i\omega t), \quad (19)$$

where $\eta = \text{Ga}$ if there is a Ga atom at the j th position, and $\eta = \text{As}$ if at the j th position there is an As atom. Using (1) we derive from U_j , U_{j+1} , and U_{j+2} the relation

$$G_{\omega, \text{As}}^{\pm} = [(1 - \frac{1}{2}M_{\text{Ga}}\omega^2)/\cos\kappa_{\text{Ga}}]G_{\omega, \text{Ga}}^{\pm}. \quad (20)$$

Similarly, for an infinite chain of AlAs, the solution

$$U_l = D_{\omega, \eta}^{\pm} \exp(\pm i\kappa_{\text{Al}} l - i\omega t), \quad \eta = \text{Al, As} \quad (21)$$

yields the relation

$$D_{\omega, \text{As}}^{\pm} = [(1 - \frac{1}{2}M_{\text{Al}}\omega^2)/\cos\kappa_{\text{Al}}]D_{\omega, \text{Al}}^{\pm} \quad (22)$$

when U_l , U_{l-1} , and U_{l-2} are substituted into (1). Now we refer to Fig. 1(b) and study the two solutions at the interface position j_2 . Solution I is based on the AlAs chain and leads to (22), but solution II is based on the GaAs chain and (20) is valid. The uniqueness of the solution implies

$$\begin{aligned} G_{\omega, \text{As}}^+ \exp(i\kappa_{\text{Ga}} j_2) + G_{\omega, \text{As}}^- \exp(-i\kappa_{\text{Ga}} j_2) \\ = D_{\omega, \text{As}}^+ \exp(i\kappa_{\text{Al}} j_2) + D_{\omega, \text{As}}^- \exp(-i\kappa_{\text{Al}} j_2). \end{aligned} \quad (23)$$

Since in (18) the atomic positions are for As atoms only, we can rewrite $\Xi_+(\omega) + \Xi_-(\omega)$ as

$$\begin{aligned} \Xi_+(\omega) + \Xi_-(\omega) = \sum_{j \in \mathbb{R}} \{D_{\omega, \text{As}}^+ \exp[i(\kappa_{\text{Al}} - q)j] + D_{\omega, \text{As}}^- \exp[i(-\kappa_{\text{Al}} - q)j]\} \\ - \sum_{j \in \mathbb{R}} \{G_{\omega, \text{As}}^+ \exp[i(\kappa_{\text{Ga}} - q)j]\} \exp[i(\kappa_{\text{Ga}} - q)d_j] + \{G_{\omega, \text{As}}^- \exp[i(-\kappa_{\text{Ga}} - q)j]\} \exp[i(-\kappa_{\text{Ga}} - q)d_j], \end{aligned} \quad (24)$$

where d_j is the thickness of the constituent GaAs layer to the immediate right-hand side of the position j . If at a specific frequency ω all phase factors in (24) satisfy

$$\exp[i(\kappa_{\text{Ga}} - q)d_j] = \exp[i(-\kappa_{\text{Ga}} - q)d_j]$$

within a small error of the order qd_j ; then using (23), (24) becomes

$$\begin{aligned} \Xi_+(\omega) + \Xi_-(\omega) = \sum_{j \in \mathbb{R}} \{D_{\omega, \text{As}}^+ \{1 - \exp[i(\kappa_{\text{Ga}} - q)d_j]\} \exp[i(\kappa_{\text{Al}} - q)j] \\ + D_{\omega, \text{As}}^- \{1 - \exp[i(-\kappa_{\text{Ga}} - q)d_j]\} \exp[i(-\kappa_{\text{Al}} - q)j]\}. \end{aligned} \quad (24a)$$

Similarly, if we assume that at a specific frequency ω all phase factors in (24) satisfy

$$\exp[i(\kappa_{\text{Al}} - q)d_l] = \exp[i(-\kappa_{\text{Al}} - q)d_l]$$

within a small error of the order qd_l , where d_l is the thickness of the constituent AlAs layer to the immediate right-hand side of the position l , then (24) can be put in another equivalent form:

$$\begin{aligned} \Xi_+(\omega) + \Xi_-(\omega) = \sum_{l \in \mathbb{L}} \{G_{\omega, \text{As}}^+ \{\exp[i(\kappa_{\text{Al}} - q)d_l] - 1\} \exp[i(\kappa_{\text{Ga}} - q)l] \\ + G_{\omega, \text{As}}^- \{\exp[i(-\kappa_{\text{Al}} - q)d_l] - 1\} \exp[i(-\kappa_{\text{Ga}} - q)l]\}. \end{aligned} \quad (24b)$$

When $|\Xi_+(\omega) + \Xi_-(\omega)|^2$ reaches its maximum at a specific frequency ω , then from (15) and (18) we see that a peak in the Raman spectrum will be detected at the same frequency ω . The forms of (24a) and (24b) suggest the occurrence of maximum $|\Xi_+(\omega) + \Xi_-(\omega)|^2$ if all phase factors in (24a) and (24b) satisfy $(\pm\kappa_{\text{Ga}} - q)d_j = (\text{odd integer})\pi$ and $(\pm\kappa_{\text{Al}} - q)d_l = (\text{odd integer})\pi$ within a small error of the order qd_j (or qd_l). This is exactly the same conditions which lead (24) to (24a) and (24b). Under the assumption that these conditions are satisfied, (24a) and (24b) reduce simply to

$$\begin{aligned} \Xi_+(\omega) + \Xi_-(\omega) = 2 \sum_{j \in \mathbb{R}} \{D_{\omega, \text{As}}^+ \exp[i(\kappa_{\text{Al}} - q)j] \\ + D_{\omega, \text{As}}^- \exp[i(-\kappa_{\text{Al}} - q)j]\} \\ = -2 \sum_{l \in \mathbb{L}} \{G_{\omega, \text{As}}^+ \exp[i(\kappa_{\text{Ga}} - q)l] \\ + G_{\omega, \text{As}}^- \exp[i(-\kappa_{\text{Ga}} - q)l]\}. \end{aligned}$$

In each of the above forms there are two groups of terms representing the scattering of light by two degenerate vibration waves traveling in opposite directions. Therefore,

in $|\Xi_+(\omega) + \Xi_-(\omega)|^2$ the summation over the mixing terms of these two scatterings is expected to give negligible contribution. In this case we can equivalently consider the approximated formula

$$|[\Xi_+(\omega) + \Xi_-(\omega)]|^2 \approx |\Xi_+(\omega)|^2 + |\Xi_-(\omega)|^2, \quad (25)$$

where

$$|\Xi_{\pm}(\omega)|^2 = \left| \sum_{j \in R} (D_{\omega, As}^{\pm} \{1 - \exp[i(\pm \kappa_{Ga} - q)d_j]\}) \times \exp[i(\pm \kappa_{Al} - q)j] \right|^2 \quad (25a)$$

$$= \left| \sum_{l \in L} (G_{\omega, As}^{\pm} \{ \exp[i(\pm \kappa_{Al} - q)d_l] - 1 \}) \times \exp[i(\pm \kappa_{Ga} - q)l] \right|^2. \quad (25b)$$

However, the QPFSL sample considered here does not satisfy these idealized conditions. In reality, each phase factor deviates from the idealized value by a phase shift

$$\delta_{\pm, j}(\omega) = (\pm \kappa_{Ga} - q)d_j - (\text{odd integer})\pi, \quad (26a)$$

or

$$\delta_{\pm, l}(\omega) = (\pm \kappa_{Al} - q)d_l - (\text{odd integer})\pi. \quad (26b)$$

We then expect high intensity of Raman backscattering at frequencies for which the accumulated phase shift over the whole sample vanishes

$$\sum_{j \in R} \delta_{\pm, j}(\omega) + \sum_{l \in L} \delta_{\pm, l}(\omega) = 0. \quad (27)$$

We cannot prove this statement, but the ansatz (27) is justified by the following numerical results. It is important to mention that while all predicted strong Raman peaks do exist in the Raman spectrum, it does not mean that all peaks in the Raman spectrum are predicted by (27).

To calculate the sum in (27), we consider the specific QPFSL with basic building blocks $A = (\text{GaAs})_{10}/(\text{AlAs})_{10}$ and $B = (\text{GaAs})_{10}$, for which Raman backscattering data are available.¹⁸ In this system there are three different sections of constituent semiconductors: $(\text{GaAs})_{10}$, $(\text{GaAs})_{20}$, and $(\text{AlAs})_{10}$ as shown in Fig. 1(a). Let the numbers of such sections be F_{Ga1} , F_{Ga2} , and F_{Al} for $(\text{GaAs})_{10}$, $(\text{GaAs})_{20}$, and $(\text{AlAs})_{10}$, respectively. It is easy to show that $F_{Ga1} = F_{Al} - F_{Ga2}$, and for sufficiently high generation of the QPFSL system (i.e., for a sufficiently long chain) the ratio F_{Al}/F_{Ga2} approaches its limit golden mean $\tau = (\sqrt{5} + 1)/2$. If the corresponding three phase shifts are $\delta_{Ga1, \pm} = 20(\pm \kappa_{Ga} - q) - (\pm \Lambda_{Ga1})\pi$, $\delta_{Ga2, \pm} = 40(\pm \kappa_{Ga} - q) - (\pm \Lambda_{Ga2})\pi$, and $\delta_{Al, \pm} = 20(\pm \kappa_{Al} - q) - (\pm \Lambda_{Al})\pi$, where Λ_{Ga1} , Λ_{Ga2} , and Λ_{Al} are positive odd integers, then (27) leads to

$$(\tau + 1)[\kappa_{Ga}(\omega) \pm q] + \tau[\kappa_{Al}(\omega) \pm q] = [\tau(\Lambda_{Ga1} + \Lambda_{Al}) + (\Lambda_{Ga2} - \Lambda_{Ga1})]\pi/20. \quad (28)$$

$\kappa_{Ga}(\omega)$ and $\kappa_{Al}(\omega)$ are given by (17). In the low-frequency region $\kappa_{\eta}(\omega)$ can be well approximated as

$$\kappa_{\eta}(\omega) = \{[(1 + M_{\eta}/M_{As})/2]^{1/2}\}\omega, \quad \eta = \text{Ga, Al}. \quad (29)$$

Substituting $\kappa_{\eta}(\omega)$ into (28), we have

$$\omega_{\pm} = v[\frac{1}{2}(\Lambda_{Ga1} + \Lambda_{Al})\tau + \frac{1}{2}(\Lambda_{Ga2} - \Lambda_{Ga1}) \pm 10(2\tau + 1)q/\pi], \quad (30a)$$

where

$$v = (\pi/10)\{(\tau + 1)[(1 + M_{Ga}/M_{As})/2]^{1/2} + \tau[(1 + M_{Al}/M_{As})/2]^{1/2}\}^{-1}. \quad (30b)$$

If we set $M_{Ga} = M_{Al}$, then (30a) reduces to the same equation which was derived for the continuum model,^{13,18} except that in (30a) the indices to label the Raman peaks are $(\Lambda_{Ga1} + \Lambda_{Al})/2$ and $(\Lambda_{Ga2} - \Lambda_{Ga1})/2$. For given values of Λ_{Ga2} , Λ_{Ga1} , and Λ_{Al} , we calculate ω_{\pm} from (30a).

The details of numerical computations will be given in the next section. Here we will only list some results to justify the ansatz (27). If we set $\Lambda_{Ga2} = 3$ and $\Lambda_{Ga1} = \Lambda_{Al} = 1$, we can calculate ω_{\pm} from (30a) and the corresponding $\kappa_{\eta}(\omega_{\pm})$ from (29). The three phase shifts $40[\kappa_{Ga}(\omega_{-}) + q]$, $20[\kappa_{Al}(\omega_{-}) + q]$, and $20[\kappa_{Ga}(\omega_{-}) + q]$ across the constituent semiconductors $(\text{GaAs})_{20}$, $(\text{AlAs})_{10}$, and $(\text{GaAs})_{10}$ are indicated in Fig. 1(c) as angles 1, 2, and 3, respectively. The angle indicated by f in Fig. 1(c) which represents the value of the left-hand side of (28), lies just along $\theta = \pi$. Therefore, (27) is satisfied.

Since from (29) it is clear that $\kappa_{Ga} > \kappa_{Al}$, we have $\Lambda_{Ga2} > \Lambda_{Ga1} > \Lambda_{Al}$. For given values of Λ_{Ga2} , Λ_{Ga1} , and Λ_{Al} , we have computed from (30a) the corresponding ω_{\pm} and list them in Table I as $\omega_{\pm}(\text{An})$. The five integers under the first column *indices* are Λ_{Ga2} , Λ_{Ga1} , Λ_{Al} , $(\Lambda_{Ga2} - \Lambda_{Ga1})/2$, and $(\Lambda_{Ga1} + \Lambda_{Al})/2$. Exact numerical calculation of Raman tensor $R_{xx}(\omega)$ will be performed in next section. The so-derived peak positions of Raman intensity are also listed in Table I as $\omega_{\pm}(\text{Nu})$. The agreement between the analytical value $\omega_{\pm}(\text{An})$ and the exact numerical solution $\omega_{\pm}(\text{Nu})$ is very good. Nevertheless, we must point out that for the Raman peak of lowest energy, the corresponding indices $(\Lambda_{Ga2}, \Lambda_{Ga1}, \Lambda_{Al})$ are not odd integers. Very likely, for this extremely low energy the approximation (25) breaks down.

Before closing this section, we should also mention that our proposed ansatz (27) is based on (25a) and (25b) in which the effect of boundary conditions at both ends of

TABLE I. Positions of main Raman peaks predicted by the analytical solution $\omega_{\pm}(\text{An})$ and derived by the exact numerical solution $\omega_{\pm}(\text{Nu})$. The five integers under column *indices* are Λ_{Ga2} , Λ_{Ga1} , Λ_{Al} , $\frac{1}{2}(\Lambda_{Ga2} - \Lambda_{Ga1})$, and $\frac{1}{2}(\Lambda_{Ga1} + \Lambda_{Al})$. The units of ω_{\pm} are in cm^{-1} .

Indices	$\omega_{+}(\text{An})$	$\omega_{-}(\text{An})$	$\omega_{+}(\text{Nu})$	$\omega_{-}(\text{Nu})$
(2,0,0;1,0)	13.944 05	08.919 06	13.806 18	8.805 34
(1,1,1;0,1)	21.009 20	15.984 20	20.940 97	16.114 41
(3,1,1;1,1)	32.440 76	27.415 76	32.273 74	27.431 68
(5,3,1;1,2)	50.937 43	45.912 46	50.615 21	45.765 19
(7,3,1;2,2)	62.369 02	57.344 02	61.692 96	56.962 92
(5,3,3;1,3)	69.434 16	64.409 16	68.653 05	63.987 54
(7,3,3;2,3)	80.865 72	75.840 72	80.348 87	74.988 00

the sample on $D_{\omega, \text{As}}^{\pm}$ and $G_{\omega, \text{As}}^{\pm}$ are not taken into account. On the other hand, exact numerical solutions are derived with a large but finite system, where boundary conditions at both ends must be specified. We have studied the phonon mode of $\omega_- = 27.43168 \text{ cm}^{-1}$, using a 9th-generation FSL. The vibration pattern of the As subsystem is plotted in Fig. 1(d) together with the positions of interfaces marked by vertical bars along line S at the bottom. Except for the perturbation in the vicinity of each $(\text{GaAs})_{20}$ layers, the vibrational amplitude is almost constant, indicating negligible effects of the boundary conditions. In this respect, our analytical conclusion is also applicable to finite but large systems.

V. NUMERICAL SOLUTIONS IN LONG-WAVELENGTH REGION

We will perform an exact numerical study of (14) for samples with perfect sharp interfaces, and for samples with imperfection. At the end we will compare our calculations with measured Raman spectra. With the basic building blocks $S_1 \equiv A = (\text{GaAs})_{10}/(\text{AlAs})_{10}$ and $S_2 \equiv B = (\text{GaAs})_{10}$, a QPFSL is generated on computer by concatenation via the recursion relation $S_{l+2} = S_{l+1}S_l$, for $l \geq 1$. In most calculations we used 9th-generation FSL samples, but higher-generation FSL samples were also used in order to check the convergence of the calculations. Such samples have perfect sharp interfaces, and will be referred to as perfect samples. For a given sample, we solve (1) numerically to obtain the phonon spectrum and all phonon eigenmodes.

The laser light source used in the Raman scattering experiment¹⁸ has a wavelength 5145 Å, and the corresponding average refractive index of the sample is about $n = 4.7$. Therefore, we have $q \equiv 2\omega_l n / c = 0.0163$ which yields a doublet splitting of each Raman peak by $\omega_+ - \omega_- \approx 5 \text{ cm}^{-1}$. In Ref. 22 the values of the Raman polarizability are given as $\alpha_{xx, \text{Ga}} = 6.0$ and $\alpha_{xx, \text{Al}} = 1.2$. The experiment is usually done at room temperature, and so we set $T = 300 \text{ K}$. With all these specifications, the Raman intensity is calculated from (14). In the region $\omega < 100 \text{ cm}^{-1}$, the Raman spectrum of a perfect sample is shown in Fig. 2(a). The drop of the Raman intensity with increasing ω is due to the Boltzmann factor $[1 - \exp(-\hbar\omega/k_B T)]^{-1}$. The splitting of each Raman peak into a doublet is clearly seen.

In reality the QPFSL samples are not perfect. Nakayama *et al.*¹⁸ have claimed that in their samples the position of each interface is controlled within an accuracy of one monolayer. Such imperfection can be generated by computer simulation with two different methods. We can first make a perfect sample, and then displace each interface randomly by one monolayer either to the right or to the left with a probability X . Then the probability of an interface remaining at its correct position is $1 - 2X$. In this case, the imperfections at different positions are not correlated. We call this situation *independent disorder*.

For the second method, we generate the first interface with its position measured from the substrate. The probability of having correct separation between the first interface and the substrate is $1 - 2X$, and the probability of

having one monolayer either thicker or thinner than the correct thickness is X . Knowing the exact position of the first interface and using it as a reference position for measuring the thickness of the next constituent material, the second interface is simulated in a similar fashion. This procedure is repeated until the entire QPFSL is generated. In this case, the imperfections from a *correlated disorder*.

The Raman spectra of independent-disordered samples are shown in Fig. 2, and the Raman spectra of correlated-disordered samples are shown in Fig. 3. The degree of imperfection is indicated by the value of X . In both cases the effect of imperfection decreases with increasing wavelength, as one would expect. Nevertheless, by comparing Figs. 2 and 3, we still detect the difference that the correlated disorder destroys the Raman signal more effectively than the independent disorder.

When we compare our calculated Raman spectra with the measured ones of Nakayama *et al.*,¹⁸ although all measured doublet Raman peaks are reproduced by theory, the calculated peak positions are slightly lower than the corresponding measured ones. While the top edge of the longitudinal-acoustic branch is pinned by the ratio of the elastic constant K and the heavier As atomic mass M_{As} , we notice from (30a) and (30b) that in the long wavelength region the phonon frequency ω is a function of the mass ratios $M_{\text{Al}}/M_{\text{As}}$ and $M_{\text{Ga}}/M_{\text{As}}$. In our calculation we have used the bare atomic masses for M_{Ga} , M_{Al} , and M_{As} . On the other hand, in our simple one-dimensional model for a QPFSL the ratios $M_{\text{Ga}}/M_{\text{As}}$ and

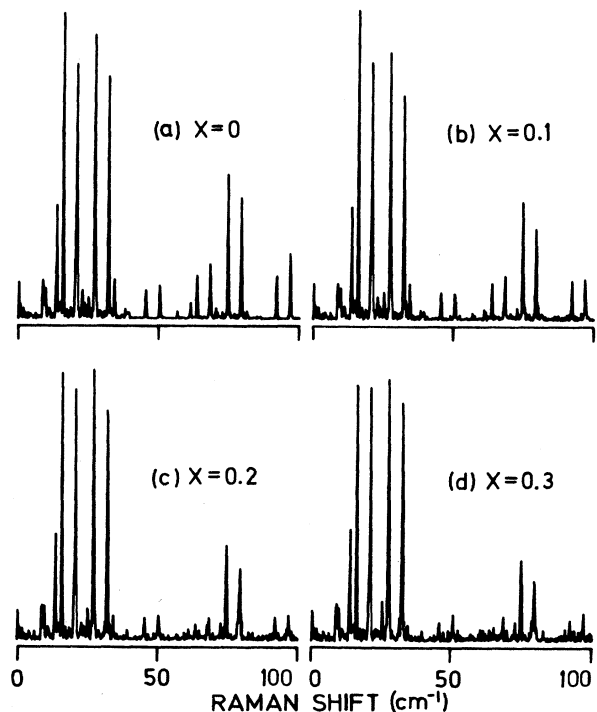


FIG. 2. Computed Raman spectra in the low-frequency region for various degrees of independent disorder specified by the value of X . All plots have same vertical scale in arbitrary units.

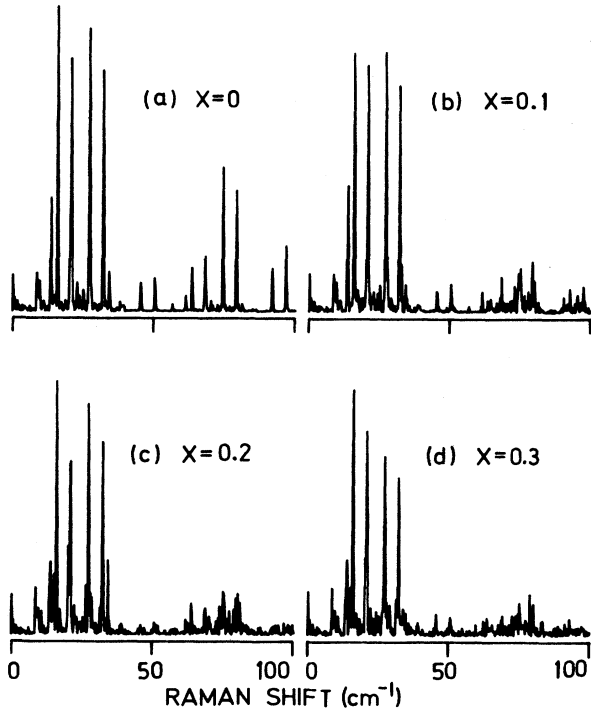


FIG. 3. Computed Raman spectra in the low-frequency region for various degrees of correlated disorder specified by the value of X . All plots have same vertical scale in arbitrary units.

M_{Al}/M_{As} should have proper effective values. If we treat M_{Ga}/M_{As} and M_{Al}/M_{As} as adjustable parameters, the low-frequency part of the longitudinal-acoustical phonon spectrum will be modified but the high-frequency part will remain practically unchanged. By reducing the ratios M_{Al}/M_{As} and M_{Ga}/M_{As} , and so increasing the long-wavelength phonon frequency ω by a factor about 1.2, our calculated Raman spectrum $(-1/\omega)R_{xx}(\omega)$ is shown in Fig. 4, together with experimental curves of Nakayama *et al.*¹⁸

In the experimental spectrum the broad maximum around $\omega=0$ is due to the elastic scattering of the incident laser light. If we subtract this elastic peak, the theoretical calculation agrees very well with the experimental observation. Each double-peak is labeled by two indices $[\frac{1}{2}(\Lambda_{Ga2}-\Lambda_{Ga1}), \frac{1}{2}(\Lambda_{Ga}+\Lambda_{Al})]$, the values of which are listed in Table I as the last two integers under the column *indices*.

Nakayama *et al.*¹⁸ have used the continuum model to calculate the Raman spectrum. Their result [Fig. 3(a) of Ref. 18] agrees with ours, except that they could not obtain the (1,2) doublet peak around $\omega \approx 55-60 \text{ cm}^{-1}$. Dharma-wardana and his co-workers^{28,29} have shown that when the structure factor of the building blocks is properly taken into account in the plane-wave approximation, via a projection from a related two-dimensional periodic structure, the continuum model should also yield this (1,2) doublet-peak around $\omega \approx 55-60 \text{ cm}^{-1}$. In the framework of our analysis, we can easily demonstrate the effect of this structure factor for the particular basic

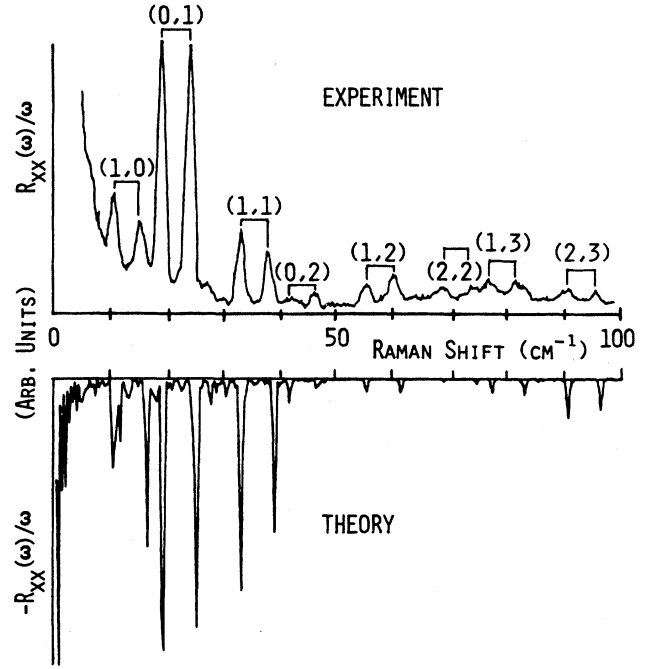


FIG. 4. Comparison of our computed Raman spectrum for a perfect QPFSL sample and the measured one from Ref. 18.

building blocks $A=(\text{GaAs})_{10}/(\text{AlAs})_{10}$ and $B=(\text{GaAs})_{10}$. Let us use simple plane waves for the phonon eigenmode. Then, within an error of the order q , (25b) reduces to

$$|\Xi_{\pm}(\omega)|^2 \propto \left| \sum_{l \in \text{CL}} [\exp(\pm i\kappa d_l) - 1] \exp(\pm i\kappa l) \right|^2. \quad (31)$$

It has been shown^{18,30} that $|\Xi_{\pm}(\omega)|^2$ is negligibly small unless

$$\pm\kappa = 2\pi(n\tau + m)/(\tau d_A + d_B), \quad (32)$$

where d_A (or d_B) is the thickness of the building block A (or B) and the integers (m, n) play the roles of our indices $[\frac{1}{2}(\Lambda_{Ga2}-\Lambda_{Ga1}), \frac{1}{2}(\Lambda_{Ga}+\Lambda_{Al})]$. For the QPFSL sample under consideration, $d_A=40$ and $d_B=20$, and for all l in (31) we have $d_l=d_A-d_B=20$. Therefore, for $m=1$ and $m=2$ we have

$$|\Xi_{\pm}(\omega)|^2 \propto \left| \sum_{l \in \text{CL}} [\exp(\pm i2\pi) - 1] \exp[i(\pm\kappa - q)l] \right|^2 = 0. \quad (33)$$

We have also checked the eigenmodes corresponding to the (1,2) peaks. The Fourier spectra of these modes clearly indicate that plane waves do not give good approximated eigenfunctions. This investigation explains the discrepancy between the calculated spectrum of Nakayama *et al.*¹⁸ and our result, Fig. 4, which agrees with the analysis of Refs. 28 and 29.

VI. FIBONACCI CHARACTERISTIC

It was first pointed by Dharma-wardana and his co-workers^{28,29} that the Raman peak positions in a QPFSL

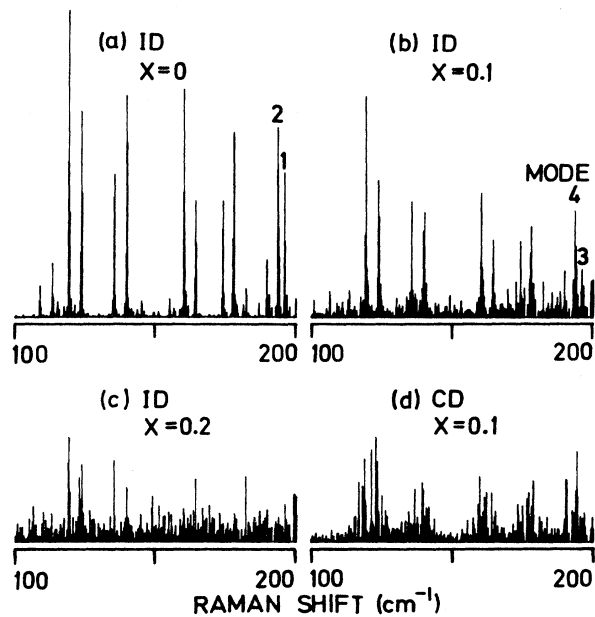


FIG. 5. Computed Raman spectra in high-frequency region for (a) a perfect QPFSL sample, (b) and (c) samples with independent-disorder, and (d) samples with correlation disorders.

sample are specified by double indices as opposed to the single-index labeling of the peak positions in a periodic superlattice. The same conclusion remains when the discrete model is used instead of the continuum model. This signature of the Fibonacci characteristics in the low-frequency Raman spectrum is clearly revealed by the excellent agreement between the theoretical calculation and the experimental data as shown in Fig. 4.

Another important feature of the Fibonacci structure is the so-called critical state. As short-wavelength phonon modes are more sensitive to the Fibonacci modulation, critical phonon modes are expected to appear near the top-edge of the longitudinal-acoustical branch. It is therefore very interesting to study the Raman spectrum in this region. Unfortunately, in reality, the Raman intensity is very weak in this frequency range owing to two reasons. The first one is the Boltzmann factor $[1 - \exp(-\hbar\omega/k_B T)]^{-1}$ in (15) which suppresses $R_{xx}(\omega)$ for large ω . The second reason is the imperfection which affects strongly eigenmodes of short wavelength.

Figure 5(a) shows the calculated Raman spectrum of a perfect QPFSL sample in the frequency region between 100 and 201 cm^{-1} (between the middle and the top edge of the acoustical branch). The doublet of each Raman peak can still be clearly resolved. When imperfection of the independent-disorder type is included, the Raman spectrum changes into Figs. 5(b) and 5(c) for $X=0.1$ and $X=0.2$, respectively. This distortion of the spectrum gets even worse for imperfection of the type of correlated disorder, as shown by Fig. 5(d) with $X=0.1$.

In order to demonstrate the effect of imperfection on eigenmodes, we selected four Raman peaks and analyzed

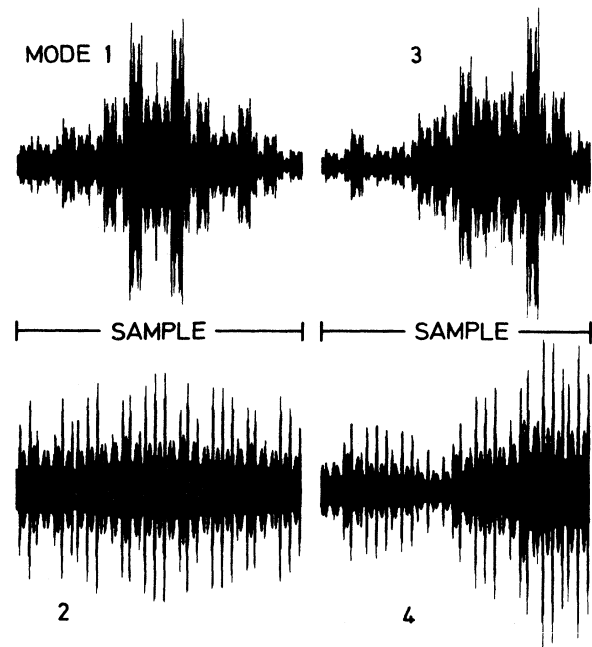


FIG. 6. Lattice vibration patterns of the four eigenmodes specified in Fig. 5.

in details their corresponding eigenfunctions. These four peaks are marked as 1, 2, 3, and 4 in Figs. 5(a) and 5(b). Figure 6 gives the vibration patterns of these eigenmodes. It is important to point out that mode 1 is the so-called critical state characteristic to the Fibonacci structure, but mode 2 is simply a normal phonon mode. However, a very weak imperfection (independent disorder with $X=0.1$) turns these two qualitatively entirely different eigenfunctions into mode 3 and mode 4, both of which are typical wave functions of a random system. In other words, the critical phonon modes of a QPFSL are easily removed by very weak imperfection at the interfaces.

To our knowledge there is no published Raman back-scattering data in the frequency range between 100 and 201 cm^{-1} . Our analysis here suggests the requirement of extremely high-quality QPFSL samples in order to explore the interesting properties of the critical eigenmodes in the Fibonacci structure. However, we must remind ourselves of the fact that the force constant of pure AIAs is slightly larger than the force constant of pure GaAs. Hence, near the top edge of the longitudinal-acoustical branch, phonons propagate in AIAs layers but decay weak exponentially in GaAs layers. As a result, in the region where critical phonon modes are expected, one may find something entirely different.

ACKNOWLEDGMENT

This work was financially supported by the Swedish Natural Science Research Council under Grant No. NFR-FFU-3996-140.

- ¹D. R. Hofstadter, *Phys. Rev. B* **14**, 2239 (1976).
- ²C. de Lange and T. Janssen, *Phys. Rev. B* **28**, 195 (1983).
- ³T. Janssen and J. A. Tjon, *Ferroelectrics* **53**, 255 (1984).
- ⁴J. B. Sokoloff, *Phys. Rev. B* **22**, 5823 (1980).
- ⁵M. Kohmoto, L. P. Kadanoff, and C. Tang, *Phys. Rev. Lett.* **50**, 1870 (1983).
- ⁶J. B. Sokoloff, *Phys. Rep.* **126**, 189 (1985).
- ⁷T. Janssen and J. A. Tjon, *Phys. Rev. B* **25**, 3767 (1982).
- ⁸G. Andre and S. Aubry, *Ann. Israel Phys. Soc.* **3**, 133 (1980).
- ⁹J. H. Avron and B. Simon, *Duke. Math. J.* **50**, 369 (1983).
- ¹⁰Th. Rasing, *Phys. Rev. Lett.* **53**, 388 (1984).
- ¹¹G. Wahlström and K. A. Chao, *Phys. Rev. B* **36**, 9753 (1987).
- ¹²R. B. Stinchcombe and S. C. Bell, *J. Phys. A* **20**, L739 (1987).
- ¹³R. Merlin, K. Bajema, R. Clarke, F.-Y. Juang, and P. K. Bhattachary, *Phys. Rev. Lett.* **55**, 1768 (1985).
- ¹⁴S. Das Sarma, A. Kobayashi, and R. E. Prange, *Phys. Rev. Lett.* **56**, 1280 (1986).
- ¹⁵P. Hawrylak and J. J. Quinn, *Phys. Rev. Lett.* **57**, 380 (1986).
- ¹⁶K. Bajema and R. Merlin, *Phys. Rev. B* **36**, 4555 (1987).
- ¹⁷J. Todd, R. Merlin, R. Clarke, K. M. Mohanty, and J. D. Axe, *Phys. Rev. Lett.* **57**, 1157 (1986).
- ¹⁸M. Nakayama, H. Kato, and S. Nakashima, *Phys. Rev. B* **36**, 3472 (1987).
- ¹⁹M. G. Karkut, J.-M. Triscone, D. Ariosa, and O. Fischer, *Phys. Rev. B* **34**, 4390 (1986).
- ²⁰M. W. C. Dharma-wardana, A. H. MacDonald, D. J. Lockwood, J.-M. Baribeu, and D. C. Houghton, *Phys. Rev. Lett.* **17**, 1761 (1987).
- ²¹C. Colvard, T. A. Gant, M. V. Klein, R. Merlin, R. Fischer, H. Morkoç, and A. C. Gossard, *Phys. Rev. B* **31**, 2080 (1985).
- ²²A. S. Barker, Jr., J. L. Merz, and A. C. Gossard, *Phys. Rev. B* **17**, 3181 (1978).
- ²³B. Zhu and K. A. Chao, *Phys. Rev. B* **36**, 4906 (1987).
- ²⁴M. Born and K. Huang, *Dynamical Theory of Crystal Lattices* (Oxford University Press, London, 1954).
- ²⁵B. Jusserand, D. Paquet, and A. Regreny, *Phys. Rev. B* **30**, 6245 (1984).
- ²⁶R. J. Bell, in *Methods in Computational Physics*, edited by B. Alder, S. Fernbach, and M. Rotenberg (Academic, New York, 1976), Vol. 15, p. 260.
- ²⁷J. He, B. Djafi-Rouhani, and J. Sapriel, *Phys. Rev. B* **37**, 4086 (1988).
- ²⁸M. W. C. Dharma-wardana, A. H. MacDonald, G. C. Aers, D. J. Lockwood, W. T. Moore, and R. L. S. Devine, *Superlatt. Microstruct.* **3**, 665 (1987).
- ²⁹D. J. Lockwood, A. H. MacDonald, G. C. Aers, M. W. C. Dharma-wardana, R. L. S. Devine, and W. T. Moore, *Phys. Rev. B* **36**, 9286 (1987).
- ³⁰D. Levine and P. J. Steinhardt, *Phys. Rev.* **34**, 596 (1986).